ACS APPLIED MATERIALS & INTERFACES

Research Article

www.acsami.org

Transparent Nanocellulosic Multilayer Thin Films on Polylactic Acid with Tunable Gas Barrier Properties

Christian Aulin,*[,†,‡] Erdem Karabulut,[§] Amy Tran,[§] Lars Wågberg,[‡,§] and Tom Lindström[†,‡]

[†]Innventia AB, Box 5604, SE-11486 Stockholm, Sweden

[‡]Wallenberg Wood Science Center, KTH Royal Institute of Technology, SE-10044 Stockholm, Sweden

[§]Fibre and Polymer Technology, KTH Royal Institute of Technology, SE-10044 Stockholm, Sweden

Supporting Information

ABSTRACT: The layer-by-layer (LbL) deposition method was used for the build-up of alternating layers of nanofibrillated cellulose (NFC) or carboxymethyl cellulose (CMC) with a branched, cationic polyelectrolyte, polyethyleneimine (PEI) on flexible poly (lactic acid) (PLA) substrates. With this procedure, optically transparent nanocellulosic films with tunable gas barrier properties were formed. 50 layer pairs of PEI/NFC and PEI/CMC deposited on PLA have oxygen permeabilities of 0.34 and 0.71 $cm^3 \cdot \mu m/m^2 \cdot day \cdot kPa$ at 23 °C and 50% relative humidity, respectively, which is in the same range as polyvinyl alcohol and ethylene vinyl alcohol. The oxygen permeability of these multilayer nanocomposites outperforms those of pure NFC films prepared by solvent-casting. The nanocellulosic LbL assemblies on PLA substrates was in detailed characterized using a quartz crystal microbalance with dissipation (QCM-D). Atomic force microscopy (AFM) reveals large structural differences between the PEI/NFC and the PEI/CMC assemblies, with the PEI/NFC assembly showing a highly entangled network of nanofibrils, whereas the PEI/CMC surfaces lacked structural features. Scanning electron microscopy images showed a nearly perfect uniformity of the nanocellulosic coatings on PLA, and light transmittance results revealed remarkable transparency of the LbL-coated PLA films. The present work demonstrates the first ever LbL films based on high aspect ratio, water-dispersible nanofibrillated cellulose, and water-soluble carboxymethyl cellulose polymers that can be used as multifunctional films and coatings with tailorable properties, such as gas barriers and transparency. Owing to its flexibility, transparency and high-performance gas barrier properties, these thin film assemblies are promising candidates for several large-scale applications, including flexible electronics and renewable packaging.

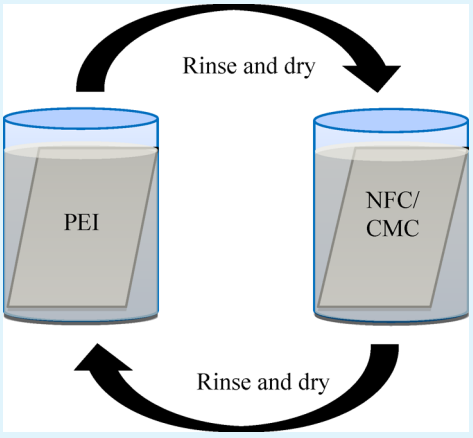

KEYWORDS: *nanocellulose, oxygen permeability, water vapor permeability, multilayer, transparency, gas barrier*

INTRODUCTION

Thin films exhibiting high gas barrier properties, effectively increasing the tortuous path for penetrating gas molecules, are essential for food packaging,[1,2] flexible electronics,[3] and fuel cells.[4] Conventional petroleum-based plastics, metalized films,[5] SiO_x coatings,[6] and clay-filled polymer composites[7−9] have all been studied for their gas barrier properties.[10] Deposited onto a flat surface, inorganic coatings, such as SiO_x, possess high gas barrier properties, but pinholes or defects are easily generated during converting operations probably due to the brittle properties of these films.[11,12] Conventional polymer composites are tougher, including a higher strain-to-failure, but filler aggregation during manufacturing of the films reduces the barrier properties and decreases transparency.[10] In striving toward a sustainable society, it is critical to replace fossil-based plastics and inorganic coatings with renewable and biodegradable barrier coatings.[13] As derived from renewable resources and due to its inherent gas barrier properties, nanocellulose has achieved much attention as a promising replacement of fossil-based polymers in gas barrier applications.[14−19]

Nanocellulose, also denoted as nanofibrillated cellulose (NFC) or microfibrillated cellulose (MFC), exhibits diameters in the nanometer range and lengths up to several micrometers.[20] These native semicrystalline[21] cellulose I nanofibrils are composed of highly aligned cellulose chains strongly associated through inter- and intramolecular H-bonding and noncovalent interactions. NFC is produced using chemical, enzymatic, or mechanical pretreatment procedures followed by homogenization of wood and plants,[22−24] to form materials with a high structural strength. NFC belongs to a unique class of nanomaterials with high stiffness in the range of 29−145 GPa,[25,26] lightweight properties (density ca. 1.5 g/cm^3), and a large specific surface area, 482 m^2/g,[27] which makes the

Received: May 7, 2013
Accepted: July 8, 2013
Published: July 8, 2013

nanofibrils an ideal material for surface functionalization via different reactions. The preparation procedures, general properties, and potential future applications of NFC have been thoroughly reviewed elsewhere.[19,20,28,29]

So far, thin films of NFC with promising oxygen barrier properties have been fabricated by solvent-casting, filtering, or various coating techniques.[14−17] The preparation procedures are usually time-consuming due to a low solid content of the NFC dispersion, and hence, a large amount of water has to be evaporated to allow film formation.

The layer-by-layer (LbL) technique is a simple, efficient, robust, and water-based method for preparing thin films with multifunctional properties.[10,30−32] The technique is based on the alternative deposition of oppositely charged polymers or nanoparticles onto a substrate forming thin layers with tunable nanoscale architecture. This precisely controlled deposition of polyelectrolytes and colloids have previously been used to design gas barrier thin films with interesting properties.[10,33−39]

In the present study, the LbL technique was used to build-up novel nanocellulosic multilayered thin films using branched, cationic polyethylenimine (PEI) with nanofibrillated cellulose (NFC) or carboxymethyl cellulose (CMC) on polylactic acid (PLA) substrates. PLA was selected as substrate due to its renewability and biodegradability and since it is conceived to be a potential replacement for commercial fossil-based materials in packaging applications.[36] The nanocellulosic thin film assembly includes good functional properties such as remarkable oxygen barrier properties and optical transparency when deposited on PLA films.

EXPERIMENTAL SECTION

Materials. Branched polyethyleneimine (PEI) (M_w = 25 000 g/mol, M_n = 10 000 g/mol) was purchased from Sigma Aldrich (Germany). Aqueous PEI solutions, 1 g/L and pH = 10.2, were prepared using Milli-Q water and stirred using a magnetic stirrer for 24 h.

The anionic NFC used in this study was prepared by modification of a previously described procedure[23] using a carboxymethylation[24] pretreatment of the fibers. Experimental details for the preparation of anionic NFC can be found elsewhere[22,24] and are only briefly described here. A dissolving pulp (Domsjö dissolving plus, Domsjö Fabriker, Sweden) was dispersed in deionized water followed by solvent exchange to ethanol and impregnation in a solution of monochloroacetic acid in isopropanol. The fibers were then filtered and washed with deionized water and acetic acid. Finally, the fibers were impregnated with a $NaHCO_3$ solution in order to convert the fibers into their sodium form to further enhance cell wall delamination. Following the carboxymethylation step, the fibers were passed through a high-pressure homogenizer (Microfluidizer M-110EH, Mircofluidics Corp). The homogenizer was equipped with a chamber pair with a diameter of 200 and 100 μm, respectively, and the operating pressure was 1700 bar. To ensure a completely delamination of the fibers into individual nanofibers, the suspension was homogenized six times, each with a subsequent dilution step. The final concentration of the nanofiber dispersion was 0.1 wt %. Such a procedure leads to the liberation of cellulose I nanofibers, mostly with a diameter of 5−20 nm and lengths of a few micrometers.[22] The total charge density of the highly carboxymethylated NFC dispersion was measured to be 627 meq/g[24] by conductometric titration. This corresponds to a degree of substitution of the cellulose of 0.1.

Carboxymethyl cellulose (CMC) (M_w = 250 000 g/mol) was purchased from Sigma Aldrich (Germany). Aqueous CMC solutions, 1 g/L and pH = 6.4, were prepared using Milli-Q water and stirred using a magnetic stirrer for 24 h.

Poly (lactic acid) (PLA), Ingeo 4060D, was kindly supplied by NatureWorks LLC. According to the supplier, the PLA resin is of amorphous character with a T_g of 55−60 °C.

Preparation of Multilayered PLA Films. PLA films were melt pressed using a Polystat 200 T (Servitec, Germany) at 300 bar and at a temperature of 165 °C. The resulting films had a thickness of 113 ± 3 μm.

Before use, the PLA film was cleaned by first rinsing with water, then with ethanol, and finally with water again. This procedure was followed by a plasma oven treatment for 3 min (PDC-002, Harrick Scientific Incorp, US) operating at 30 W under reduced air pressure in order to make the surfaces hydrophilic.

Each treated PLA substrate was first dipped into a PEI solution (5 min) followed by rinsing with deionized water and then drying. The same procedure was then used for the deposition of NFC or CMC. This deposition method was repeated until the desired number of bilayers was obtained. Figure 1 shows a schematic drawing of the layer-by-layer deposition process. Both sides of the PLA substrate are being coated using this deposition mode. Unless otherwise stated, the number of bilayers given for a LbL-coated PLA film always refers to the number of bilayers on one side of the film. The adsorption of the different components to the PLA substrate was characterized using the quartz crystal microbalance with dissipation (QCM-D) technique in model experiments.

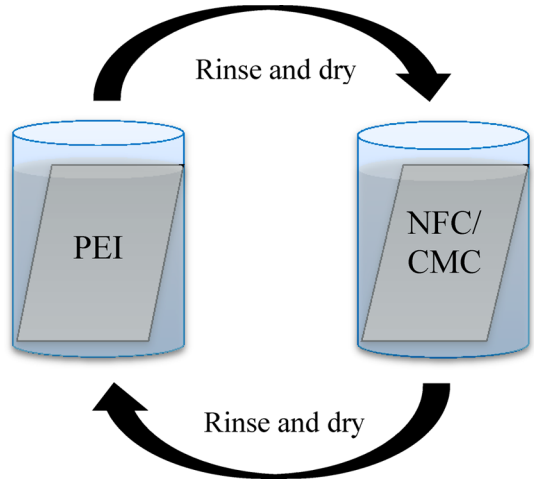

Figure 1. Layer-by-layer deposition process with cationic polyethyleneimine (PEI) and anionic nanofibrillated cellulose (NFC) or carboxymethyl cellulose (CMC) on the PLA substrate. Schematic drawing is based on ref 34.

DETERMINATION OF ADSORBED AMOUNTS AND CHARACTERIZATION OF THE FORMED LAYERS

Quartz Crystal Microbalance with Dissipation (QCM-D). A quartz crystal microbalance with dissipation (QCM-D) supplied by Q-sense AB (Västra Frölunda, Sweden) was used to study the formation of the nanocellulose-based multilayers on PLA-covered silica crystals. A detailed description of the QCM-D technique is available as Supporting Information. Prior to measurements, the PLA was dissolved in chloroform (>99%, Merck, Germany) at a concentration of 5 g/L followed by spin-coating onto the QCM crystals using a spin-coater (KW-4A, Chemat Technology, UK), and the spinning speed was 3500 rpm. After the spin coating, the PLA film was cleaned by first rinsing with water, then with ethanol, and finally with water again. This procedure was followed by a plasma oven treatment for 3 min (PDC-002, Harrick Scientific Incorp, US) operating

at 30 W under reduced air pressure in order to make the surfaces hydrophilic.

Atomic Force Microscopy (AFM) Imaging. AFM (Picoforce SPM; Veeco, Santa Barbara, CA) imaging was used to characterize the surface morphology and surface roughness of the LbL assembly films. These images were scanned in tapping mode under ambient air conditions (23 °C and 50% relative humidity). The RTESP silica cantilevers (Veeco, Santa Barbara, CA) (tip radius of 8 nm and a spring constant of 40 N/m) were oscillated at their fundamental resonance frequencies ranging between 200 and 400 kHz. The roughness value was determined from the height image over a 3 × 3 μm^2 image and is presented as a root-mean-square (rms) value. No image processing except flattening was utilized.

Optical Properties. The in-line transmittance of the multilayered-coated PLA films was measured in the UV–visible region (200–800 nm) with a Shimadzu UV-2550 UV–vis spectrophotometer (Japan). The transmittance spectra were acquired using air as background.

Scanning Electron Microscopy (SEM). Cross-sectional secondary electron images of freestanding multilayer films were taken by a Hitachi S-4800 field emission scanning electron microscope (FE-SEM). Specimens were sandwiched vertically between two complementary metal plates while their lateral parts were covered with colloidal graphite adhesive tape. The thickness of the samples was measured from ten different points of the LbL film coated surface, and the average thickness was calculated.

Oxygen and Water Vapor Permeability. The oxygen transmission rate (OTR) of the LbL-coated PLA substrates was studied with a Mocon Ox-Tran Model 2/21 apparatus (Mocon, Minneapolis, USA) in accordance with ASTM D 3985-06, and the test conditions were 23 °C at 50% RH and 38 °C at 90% RH, respectively. The sample area was 5 cm^2, and the partial pressure of the oxygen was 1 atm. The OTR was normalized with respect to pressure and material thickness and converted to the oxygen permeance and oxygen permeability (OP), respectively. Three measurements were made for each film composition, and the average value is reported.

The water vapor transmission rate (WVTR) of the LbL-coated PLA substrates was studied using a Mocon Permatran 3/33 apparatus (Mocon, Minneapolis, USA) in accordance with ASTM D 3985-06, and the test conditions were 23 °C at 50% RH and 38 °C at 90% RH, respectively. The sample area was 5 cm^2, and the partial pressure of water vapor was 0.01387 and 0.05826 atm at 50 and 90% RH, respectively. The WVTR was normalized with respect to pressure and material thickness and converted to the water vapor permeance and water vapor permeability (WVP), respectively. Three measurements were made for each film composition, and the mean value is reported.

RESULTS AND DISCUSSION

Thin Film Formation, Morphology, and Optical Characterization. The primary objective with this work was to form thin and uniform LbL films of PEI with NFC or CMC onto PLA to enhance its gas barrier properties. It was hence considered to be of importance in a detailed study whether nanocellulosic LbL structures could be formed on PLA substrates.

The adsorption processes of PEI/NFC and PEI/CMC onto PLA-coated model silica crystals have been monitored in situ as a function of time using the quartz crystal microbalance with dissipation (QCM-D) technique (Figure 2).[40] The frequency and dissipation changes for the $(PEI/NFC)_5$ film was

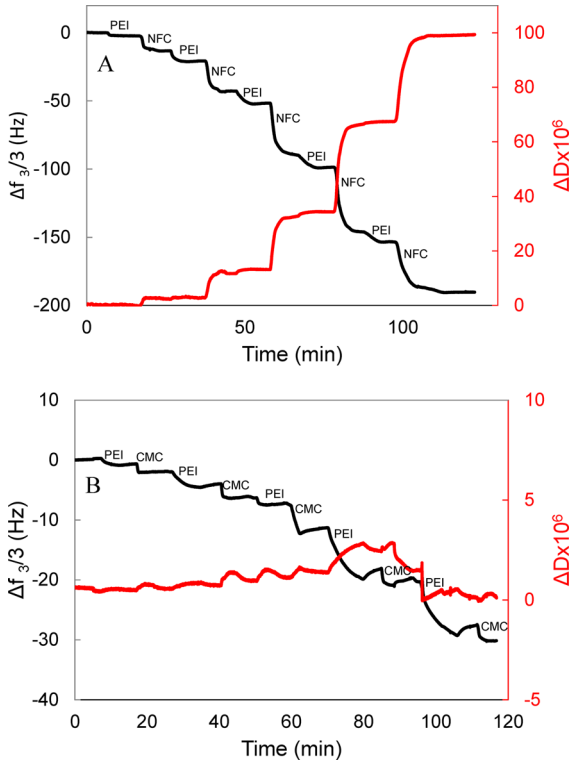

Figure 2. Representative build-up of (A) $(PEI/NFC)_5$ and (B) $(PEI/CMC)_5$ LbL films on PLA as measured with the QCM-D. The change in normalized frequency (third overtone) (left axis) and the change in energy dissipation (right axis) is shown. Each adsorption step is indicated by the name of the added component.

significantly larger than that for the LbL film prepared from the PEI and CMC. The $(PEI/CMC)_5$ assembly exhibited almost unchanged dissipation valued throughout the multilayer build-up. The formation of such viscoelastic (soft) layers is associated with a highly entangled nanofibril network enriched with large amounts of water, which have been characterized in detail earlier by QCM-D and DPI, respectively.[22,41] The high aspect ratio of the nanofibrils in combination with its comprehensive entanglement in the layer-by-layer assembly results in significant gelation. A photo highlighting the appearance of 150 bilayers on a silicon wafer and its corresponding gel-like structure is available in the Supporting Information.

In Figure 3, the frequency change was converted to the sensed mass of the individual layers and the total mass of the multilayer films using the Sauerbrey model.[42] The total mass of the $(PEI/NFC)_5$ and the $(PEI/CMC)_5$ multilayer films, including immobilized water, was calculated to be ca. 33 and 5 mg/m^2. These calculations assume that the multilayer has a homogeneous and uniform morphology and should be taken as estimates. The results clearly show that it is possible to form LbL structures on the PLA surfaces, and they also show that the adsorbed mass of $(PEI/NFC)_5$ is somewhat lower than previous findings of Aulin et al.[41] and Karabulut et al.,[43] where the adsorbed masses for $(PEI/NFC)_5$ films on silica were found to be ca. 55 and 52 mg/m^2, respectively. This can be attributed to the fact that the adsorption of LbL components is significantly dependent on the amount of charged groups of the

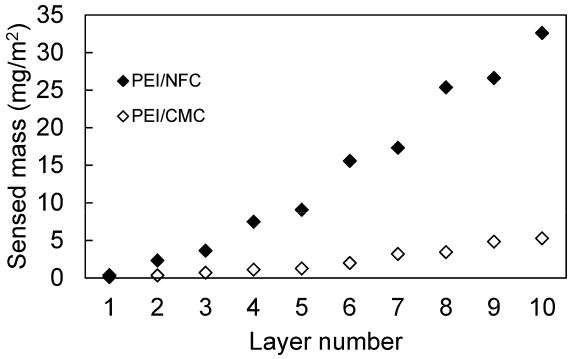

Figure 3. Total adsorbed mass of the $(PEI/NFC)_5$ and $(PEI/CMC)_5$ multilayer films on the PLA surfaces from the QCM-D measurements calculated using the Sauerbrey model which includes the immobilized water inside the LbL film.

base substrates, and it is therefore assumed that the silica surfaces exhibit a higher surface charge density than the plasma-treated PLA substrates. According to the Sauerbrey model, $(PEI/NFC)_5$ has 80 wt % NFC, while $(PEI/CMC)_5$ has 48 wt % CMC of the total mass of the entire film.

The surface morphologies of the dry $(PEI/NFC)_5$ and $(PEI/CMC)_5$ films on PLA precoated silica crystals were monitored by tapping-mode AFM imaging. AFM height image of the $(PEI/NFC)_5$ film show a network structure with monodispersed fibrils and an average rms roughness of 7.0 nm, determined from 3 × 3 μm^2 areas (Figure 4B). In agreement

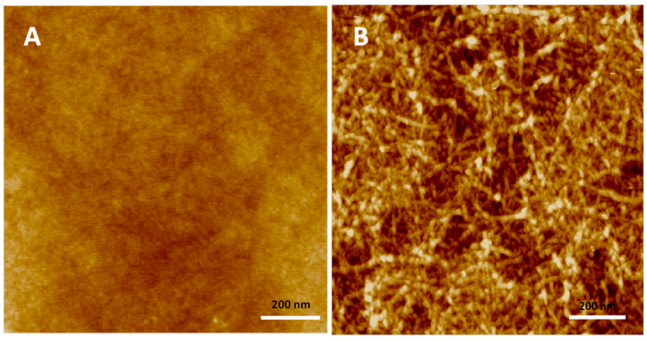

Figure 4. AFM height images of (A) $(PEI/CMC)_5$ and (B) $(PEI/NFC)_5$ films. The scanned area was 3 × 3 μm and the z range is 4 and 80 nm, respectively. The scale bar is 200 nm for both images.

with earlier AFM studies,[21,22,24] these nanofibrils appear as semiflexible with a rather constant diameter of 4 nm, taking into account the broadening effect due to the geometry of the tip. Earlier published TEM micrographs show a nanofibril diameter of about 5−15 nm.[24,44] The nanofibrils fully cover the PLA surface with no intermediate space in-between them. The $(PEI/CMC)_5$ films had a rms roughness value of 0.6 nm (Figure 4A), and no structural features could be observed. The high-charged polymer combination of PEI/CMC may contribute to such low rms roughness values. A previous study by Yang at al.[37] has shown that the surface roughness of PEI/PAA assemblies can be tailored simply by changing the charge density of each polymer and the outermost layer, resulting in thin films of these components with very low surface roughness values. AFM surface roughness profiles of $(PEI/NFC)_5$ and $(PEI/CMC)_5$ films is available as Supporting Information.

Cross-sectional SEM images of multilayer-coated PLA films were captured to measure the thickness of the LbL assemblies on the PLA substrates. In Figure 5, the SEM micrographs show

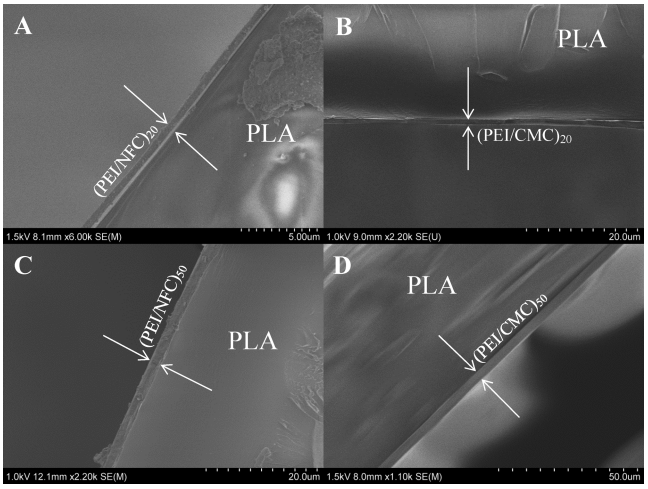

Figure 5. SEM cross-sectional images showing (A) $(PEI/NFC)_{20}$, (B) $(PEI/CMC)_{20}$, (C) $(PEI/NFC)_{50}$, and (D) $(PEI/CMC)_{50}$ assemblies on one side of the PLA. The bars highlight the thickness of the assembled films.

20 and 50 bilayers of PEI/NFC and PEI/CMC deposited on one side of a PLA film. The images demonstrate a high level of coating uniformity. High-resolution SEM images of a $(PEI/NFC)_{150}$ free-standing film were previously published by Karabulut and Wågberg[45] showing a stratified structure of the LbL components where NFC is relatively rigid or crystalline. Layer-like structures of inorganic clay and polyelectrolytes have also been shown by Priolo et al.[34] A high level of intermixing[37] and diffusion between amorphous polymers in a LbL film, such as PEI and CMC, eliminates the boundaries between each layer. It is therefore difficult to see such a layered structure for amorphous layers using SEM. From the SEM measurements, it was estimated that the thickness of 20 bilayers of PEI/NFC and PEI/CMC was 550 and 844 nm, respectively, whereas the thickness of 50 bilayers of PEI/NFC and PEI/CMC was estimated to be 1803 and 3117 nm, respectively. The PEI/CMC assembly is accompanied with a remarkable increase in thickness with deposited layers. It is conceived that this system exhibits exponential growth typical of weak polyelectrolytes similar to PAH/PAA systems.[46,47] The growth of PEI/PAA assemblies has also been thoroughly studied by Yang et al. using ellipsometry.[37,38] A 30 bilayer PEI/PAA assembly prepared from PEI at pH 10 and PAA at pH 4, respectively, resulted in a multilayer thickness of 4.74 μm. The authors demonstrated that the first few bilayers of deposition resulted in a slow growth (1−4 bilayers). After several layers are deposited, a polyelectrolyte interdiffusion mechanism dominates, resulting in rapid growth (>4 bilayers).[37,38]

Remarkable optical transparency was obtained for the thin film LbL assemblies on PLA (Figure 6). The transparency was found to be very close to that of the pure PLA film, with only minor decrease in transmittance with increased number of bilayers. Similar results were obtained by Svagan et al. using montmorillonite-based multilayers on PLA.[36] Furthermore, UV−vis spectroscopy reveals that these films exhibit promising transparency through the visible light spectrum (390−750 nm) (Figure 6). For example, the light transmittance at 600 nm for

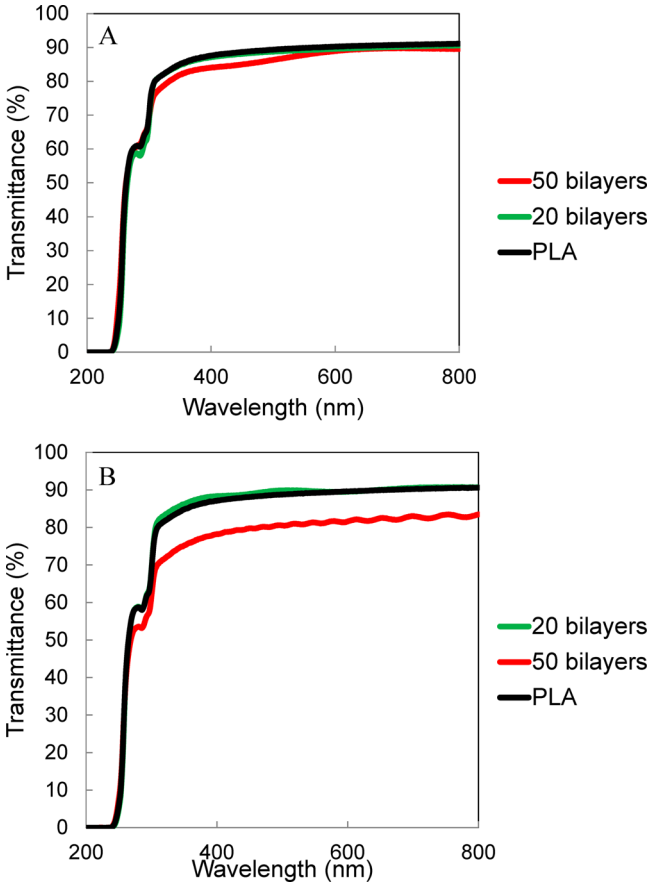

Figure 6. Light transmittance results for PLA film and PLA films on each side coated with 20 and 50 bilayers of (A) PEI/CMC and (B) PEI/NFC. The thickness was ca. 113 μm for all films.

pure PLA was 90.3%. A PLA substrate coated with 20 bilayers of PEI/NFC and PEI/CMC on each side exhibited a transparency of 88.9 and 90.4%, respectively, at 600 nm. The transparency for the PLA substrate coated with 50 bilayers of PEI/NFC is somewhat lower than that with 50 bilayers of PEI/CMC. The densely packed and amorphous characteristics of the PEI/CMC assembly result in unchanged light transmittance with respect to the number of deposited bilayers. The PEI/NFC assembly might include some minor nanofibril aggregation resulting in surface light scattering and a slightly lower light transmittance.[3]

Gas Barrier Properties. The oxygen permeance and water vapor permeance of PEI/NFC and PEI/CMC films deposited on PLA substrates measured at 23 °C and 50% RH are displayed in Figure 7. The oxygen permanence decreases with increasing number of deposited bilayers. The oxygen permeance was measured to 49.3 cm^3/m^2·day·atm for the PLA coated with 20 bilayers of (PEI/NFC) compared with 151.5 cm^3/m^2·day·atm for the uncoated PLA. The oxygen permeance was further decreased to 9.0 cm^3/m^2·day·atm when the number of deposited layers was increased to 50 (Figure 7A). The PEI/CMC assemblies exhibit the same decreasing oxygen permeance trend as PEI/NFC. A $(PEI/CMC)_{50}$ film reduces the oxygen permeance approximately 1 order of magnitude relative to the uncoated PLA substrate (Figure 7B). A 20 bilayer PEI/NFC coating deposited on PLA, which has a water vapor permeance of 4.8 g/m^2·day·atm, exhibited a water vapor permeance improvement of ca. 30%, whereas a 50 bilayer coating reduces the water vapor permeance by approximately 50% (Figure 7C). Similar trends were also observed for the PEI/CMC assemblies (Figure 7D).

Table 1 shows the thickness, oxygen, and water vapor permeabilities of the PEI/NFC and PEI/CMC assemblies. As earlier described, the LbL deposition mode used to build-up these films results in both sides of the PLA substrate being coated. The total permeability and the permeability for the decoupled assemblies in Table 1 refer to double-sided coated films.

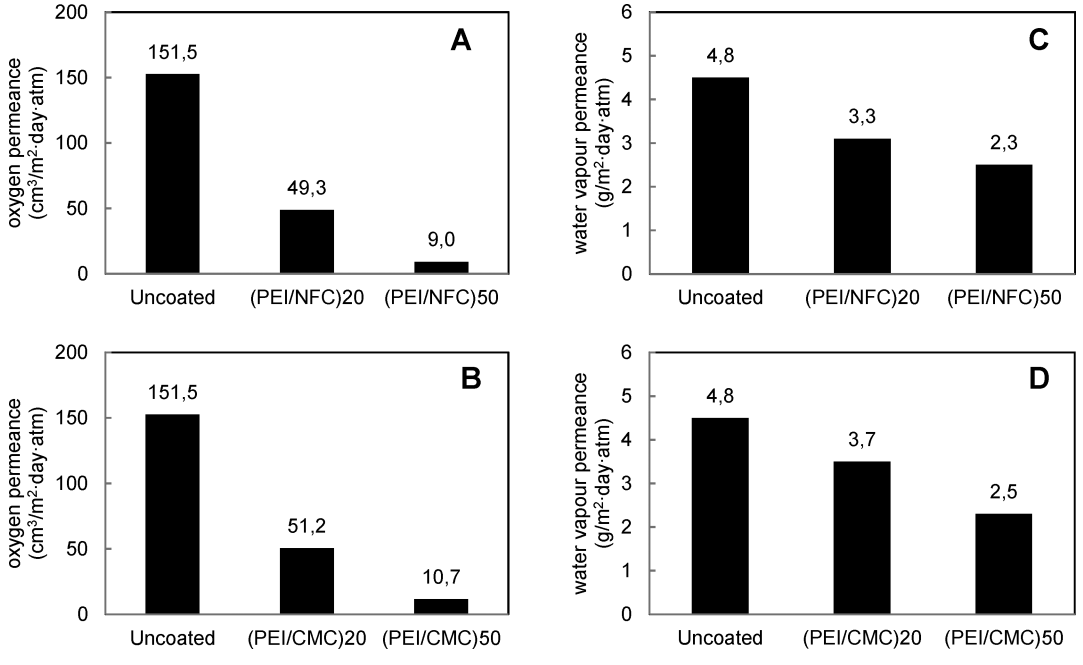

Figure 7. Oxygen permeance and water vapor permeance of (A, C) PEI/NFC and (B, D) PEI/CMC assemblies on PLA, measured at 23 °C and 50% RH. The data are mean values. Figure format is based on ref 10.

Table 1. Thickness, Oxygen, and Water Vapor Permeability Data for the PEI/NFC and PEI/CMC Assemblies at 23 °C and 50% RH[a]

	assembly thickness (nm)[b]	oxygen permeance (cm^3/m^2·day·atm)	oxygen permeability (cm^3·μm/m^2·day·kPa)		water vapor permeance (g/m^2·day·atm)	water vapor permeability (pg·m/m^2·s·kPa)	
			assembly[c]	total		assembly[c]	total
113 μm PLA		151.5		169.0	4.8		62.0
$(PEI/NFC)_{20}$	550	49.3	0.79	55.5	3.3	1.3	43.0
$(PEI/NFC)_{50}$	1803	9.0	0.34	10.2	2.3	1.8	30.6
$(PEI/CMC)_{20}$	844	51.2	1.29	58.0	3.7	3.1	48.2
$(PEI/CMC)_{50}$	3117	10.7	0.71	12.6	2.5	3.7	34.0

[a]The data are mean values. [b]Assembly thickness based on single-layer coating. [c]The water and oxygen permeabilities for the individual LbL coatings were decoupled from the total permeability.[49] Table format is based on ref 10.

Remarkable decreases in oxygen permeability with increased number of bilayers were observed for the PEI/NFC and PEI/CMC coated PLA substrates. Decoupled 50 bilayer assemblies of PEI/NFC and PEI/CMC on PLA exhibited OPs of 0.34 and 0.71 cm^3·μm/m^2·day·kPa, respectively, which is within the same range as poly (vinyl alcohol) and ethylene vinyl alcohol films.[48] These thin films are also shown to exhibit one of the lowest oxygen permeabilities reported for biobased materials. Similar results have been obtained from nanoclay-reinforced nanofibrillated cellulose films.[15,18] Compared with some commercial packaging materials, the oxygen permeability of the multilayer films is orders of magnitude lower than 427 cm^3·μm/m^2·day·kPa reported for high-density polyethylene (HDPE) and 15.6 cm^3·μm/m^2·day·kPa reported for a typical polyester.[2] Table 2 shows the oxygen permeability of the PEI/NFC and PEI/CMC assemblies compared with literature values for various biobased and synthetic polymers.

Table 2. Oxygen Permeability Data at 23 °C and 50% RH for Layer-by-Layer Assemblies of PEI/NFC and PEI/CMC and Other Published Data on Some Renewable and Synthetic Polymers

material	oxygen permeability (cm^3·μm/m^2·day·kPa)
$(PEI/NFC)_{50}$ assembly	0.34
$(PEI/CMC)_{50}$ assembly	0.71
NFC (carboxymethylated)[15]	0.52
poly(vinyl alcohol)[48]	0.21
ethylene vinyl alcohol[48]	0.30
high-density polyethylene[2]	427
amylopectin (glycerol 40 wt %)[48]	14
amylose (glycerol 40 wt %)[48]	7
O-acetyl-galactoglucomannan[14]	2.0

The present study highlights the potential of the LbL technique, which allows for the fabrication of thin film coatings with nanometer-scale architecture and a careful tuning of the gas barrier properties. It is also demonstrated that high performance barrier films can be fabricated by using all-polymer-based components, PEI/CMC, as well as water dispersible nanoparticles, PEI/NFC. The use of a LbL technique for the fabrication of high performance gas barrier films has been demonstrated by several authors before[10,33,35,37] and is not limited to cellulosic systems. The LbL technique is a water-based deposition method that previously has been used to produce super gas barrier films based on nanoclay.[33−35] Nanoclay alignment and high loading in these films is essential for generating super barrier properties, which are not possible to produce by conventional polymer composites due to filler aggregation.[35] The LbL concept presented here is environmentally friendly, water-based, and energy-efficient and is ready to be scaled up through various roll-to-toll processes, for example, simply through a multiple dipping and drying process.

The remarkable oxygen barrier properties of the PEI/NFC films is conceived to be a result from the increased tortuous path created by the high-aspect ratio impermeable semicrystalline[21] nanocellulose particles in combination with a highly densed film structure obtained by the LbL-assembly process. In addition, PEI is known to strongly intact with NFC as previously reported by Wågberg and co-workers.[24,41] PEI is a highly charged and branched molecule known for its globular structure in water and might be able to penetrate into the voids of the highly swollen NFC fibril film.[50,51] Previous studies indicate that PEI strongly adsorbs to the nanofibrils[41] and that PEI can be used as a wet-strength agent.[52] These factors allow for the formation of PEI/NFC films with improved oxygen barrier performance compared with pure NFC films prepared from solvent-casting, exhibiting an oxygen permeability of 0.52 cm^3·μm/m^2·day·kPa.[15] The LbL technique used for the fabrication of NFC-based films hence possesses an advantage over NFC films prepared from solvent-casting.

For the PEI/CMC assembled films, a high cohesive energy density, i.e., strong electrostatic interactions, intermolecular H-bonding, and van der Waals interactions, in combination with a very low polymer free volume result in high oxygen barrier properties. Similar conclusions were drawn by Gua et al.[39] and Yang et al.[37] for PEI/alginate and PEI/PAA assemblies, respectively.

A decoupled 50 bilayer PEI/NFC assembly exhibits approximately 50% lower OP than the corresponding 50 bilayer PEI/CMC assembly. This might be a result from the impermeable crystalline domains of the NFC. The crystallinity of NFC has previously been determined to be ca. 62% by XRD,[21] whereas CMC lacks any crystalline ordering. Crystalline structures are known to be impermeable toward gases.[14]

The OP at 38 °C and 90% RH was measured for neat PLA to be 290 cm^3·μm/m^2·day·kPa, and a coated PLA film with 50 bilayers of PEI/NFC had an OP of 219 cm^3·μm/m^2·day·kPa. Finally, the LbL with 50 bilayers of PEI/CMC showed an OP of 212 cm^3·μm/m^2·day·kPa. Decoupled 50 bilayer assemblies of PEI/NFC and PEI/CMC on PLA exhibited OPs of 20.8 and 36.0 cm^3·μm/m^2·day·kPa, respectively. The oxygen barrier

properties of these LbL assemblies could be improved by increasing the number of bilayers or by adsorbing a moisture-protective layer onto the surface through different cross-linking routes.[9,37,38,53] Nanoclay-based multilayer coatings result in better oxygen barrier properties at high relative humidities due to densely packed, highly aligned nanoclay structures.[35] The increased OP of the nanocellulosic LbL coatings at elevated RH is likely caused by moisture sorption and the corresponding plasticizing effect on PEI and the cellulose components. Moisture sorption decreases the molecular interaction between PEI and NFC/CMC resulting in an increased polyelectrolyte and nanofibril mobility in the LbL film. For biobased polymer films, in general, low OP at moderate relative humidities are explained by their high cohesive energy density, i.e., intra- and intermolecular hydrogen bonding and noncovalent interactions.[14] Previous studies have shown that moisture disrupts the nanofibril−nanofibril joint formation and the OP exponentially increases at high RH.[14] Nevertheless, the OP for decoupled 50 bilayer assemblies of PEI/NFC and PEI/CMC is an order of magnitude lower than that of a pure NFC film at 23 °C and 80% RH (454 $cm^3 \cdot \mu m/m^2 \cdot day \cdot kPa$).[15]

LbL gas barrier films have been mostly studied for their oxygen barrier properties, whereas water vapor permeability studies on such systems are very rare.[35] Despite hydration and swelling of the charged domains of PEI and the cellulose components and surface water trapped in the films, 50 bilayers of PEI/NFC and PEI/CMC on PLA exhibited WVP improvements of ca. 52 and 48%, respectively (Table 1). Decoupled, 50 bilayer assemblies of PEI/NFC and PEI/CMC on PLA exhibited WVPs of 1.8 and 3.7 $pg \cdot m/m^2 \cdot s \cdot kPa$, respectively. These improvements in water vapor barrier are promising for films created from dilute, aqueous nanocellulosic dispersions and solutions. A pristine NFC film exhibited a water vapor permeability of 45.7 $pg \cdot m/m^2 \cdot day \cdot atm$, whereas amylose- and amylopectin-based starch with permeability of 1.2 and 1.4 $ng \cdot m/m^2 \cdot s \cdot kPa$, respectively,[54] and cellophane (regenerated cellulose) with a permeability of 69 $ng \cdot m/m^2 \cdot s \cdot kPa$[55] have been reported. It is conceived that the high crystallinity of NFC[21] in combination with the dense structured multilayers created by the LbL process results in a moisture-resistant barrier structure. Table 3 shows the water vapor permeability of the PEI/NFC and PEI/CMC assemblies compared with literature values for various biobased and synthetic polymers.

The WVPs for the LbL-coated PLA films were also evaluated at 38 °C and 90%. For pure PLA, the WVP was measured to be 727 $pg \cdot m/m^2 \cdot s \cdot kPa$. A slight decrease in WVP was observed as a function of the number of deposited bilayers, with values of 584 and 613 $pg \cdot m/m^2 \cdot s \cdot kPa$ recorded when 50 bilayers of PEI/NFC and PEI/CMC were applied, respectively. Decoupled 50 bilayer assemblies of PEI/NFC and PEI/CMC on PLA exhibited WVPs of 81.6 and 159.6 $pg \cdot m/m^2 \cdot s \cdot kPa$ 38 °C and 90% RH, respectively.

Table 3. Water Vapor Permeability Data at 23 °C and 50% RH for Layer-by-Layer Assemblies of PEI/NFC and PEI/CMC and Literature Values for Some Renewable and Synthetic Polymers

material	water vapor permeability ($pg \cdot m/m^2 \cdot s \cdot kPa$)
$(PEI/NFC)_{50}$ assembly	1.8
$(PEI/CMC)_{50}$ assembly	3.7
NFC (carboxymethylated)[15]	45.7
arbinoxylan[56]	201
amylose[54]	1200
amylopectin[54]	1400
cellophane (regenerated cellulose)[55]	69 000

CONCLUSIONS

Thin film assemblies of PEI/NFC and PEI/CMC were adsorbed on PLA substrates using the LbL technique. QCM-D measurements showed that PEI/NFC and PEI/CMC bilayers successfully can be deposited onto PLA substrates with an increased adsorbed mass as a function of the number of bilayers. Scanning electron microscopy revealed a nearly perfect uniformity of the nanocellulosic coatings on PLA, and light transmittance measurements showed high transparency of the LbL-coated PLA films.

The resulting LbL-coated PLA films showed significantly increased oxygen and water vapor barrier properties. PLA films coated with 50 bilayers of PEI/NFC and PEI/CMC exhibited oxygen permeances that were more than an order of magnitude lower than uncoated PLA at 23 °C and 50% RH. The LbL-coated PLA substrates were also found to be less moisture sensitive compared with pure PLA, and the LbL coating significantly improved the water vapor permeance of PLA.

ASSOCIATED CONTENT

Supporting Information

Theory of quartz crystal microbalance with dissipation, a photo showing 150 bilayers of PEI/NFC deposited on a silicon wafer, and AFM surface roughness profiles of $(PEI/CMC)_5$ and $(PEI/NFC)_5$ films. This information is available free of charge via the Internet at http://pubs.acs.org/.

AUTHOR INFORMATION

Corresponding Author

*Tel.: +46-8-6767260. Fax: +46-8-4115518. E-mail: christian.aulin@innventia.com.

Notes

The authors declare no competing financial interest.

ACKNOWLEDGMENTS

The authors wish to thank the Wallenberg Wood Science Center for financial support.

REFERENCES

(1) Krochta, J. M.; De Mulder-Johnston, L. C. *Food Technol. (Chicago, IL, U.S.)* **1997**, *51*, 61−74.
(2) Miller, K. S.; Krochta, J. M. *Trends Food Sci. Technol.* **1997**, *8*, 228−237.
(3) Nogi, M.; Iwamoto, S.; Nakagaito, A. N.; Yano, H. *Adv. Mater.* **2009**, *20*, 1−4.
(4) Paula, D. R.; Robeson, L. M. *Polymer* **2008**, *49*, 3187−3204.
(5) Jamieson, E. H. H.; Windle, A. H. *J. Mater. Sci.* **1983**, *18*, 64−80.
(6) Leterrier, Y. *Prog. Mater. Sci.* **2003**, *48*, 1−55.
(7) Möller, M.; Kunz, D.; Lunkenbein, T.; Sommer, S.; Nennemann, A.; Breu, J. *Adv. Mater.* **2012**, *24*, 2142−2147.
(8) Ward, W. J.; Gaines, G. L.; Alger, M. M.; Stanley, T. J. *J. Membr. Sci.* **1991**, *55*, 173−180.
(9) Walther, A.; Bjurhager, I.; Malho, J.-M.; Pere, J.; Ruokolainen, J.; Berglund, L. A.; Ikkala, O. *Nano Lett.* **2010**, *10*, 2742−2748.
(10) Yang, Y.-H.; Bolling, L.; Priolo, M. A.; Grunlan, J. C. *Adv. Mater.* **2013**, *25*, 503−508.
(11) Barkera, C. P.; Kochemb, K.-H.; Revellc, K. M.; Kellyc, R. S. A.; Badyal, J. P. S. *Thin Solid Films* **1995**, *259*, 46−52.

(12) Leterrier, Y. *Prog. Mater. Sci.* **2003**, *48*, 1−55.
(13) Rochman, C. M.; Browne, M. A.; Halpern, B. S.; Hentschel, B. T.; Hoh, E.; Karapanagioti, H. K.; Rios-Mendoza, L. M.; Takada, H.; Teh, S.; Thompson, R. C. *Nature* **2013**, *494*, 169−171.
(14) Aulin, C.; Gällstedt, M.; Lindström, T. *Cellulose* **2010**, *17*, 559−574.
(15) Aulin, C.; Salazar-Alvarez, G.; Lindström, T. *Nanoscale* **2012**, *4*, 6622−6628.
(16) Fukuzumi, H.; Saito, T.; Iwata, T.; Kumamoto, Y.; Isogai, A. *Biomacromolecules* **2009**, *10*, 162−165.
(17) Syverud, K.; Stenius, P. *Cellulose* **2009**, *16*, 75−85.
(18) Wu, C.-N.; Saito, T.; Fujisawa, S.; Fukuzumi, H.; Isogai, A. *Biomacromolecules* **2012**, *13*, 1927−1932.
(19) Lavoine, N.; Desloges, I.; Dufresne, A.; Bras, J. *Carbohydr. Polym.* **2012**, *90*, 735−764.
(20) Klemm, D.; Kramer, F.; Moritz, S.; Lindström, T.; Ankerfors, M.; Gray, D.; Dorris, D. *Angew. Chem., Int. Ed.* **2011**, *50*, 5438−5466.
(21) Aulin, C.; Ahola, S.; Josefsson, P.; Nishino, T.; Hirose, Y.; Österberg, M.; Wågberg, L. *Langmuir* **2009**, *25*, 7675−7685.
(22) Aulin, C.; Johansson, E.; Wågberg, L.; Lindström, T. *Biomacromolecules* **2010**, *11*, 872−882.
(23) Pääkkö, M.; Ankerfors, M.; Kosonen, H.; Nykänen, A.; Ahola, S.; Österberg, M.; Ruokolainen, J.; Laine, J.; Larsson, P. T.; Ikkala, O.; Lindström, T. *Biomacromolecules* **2007**, *8*, 1934−1941.
(24) Wågberg, L.; Decher, G.; Norgren, M.; Lindström, T.; Ankerfors, M.; Axnäs, K. *Langmuir* **2008**, *24*, 784−795.
(25) Iwamoto, S.; Kai, W.; Isogai, A.; Iwata, T. *Biomacromolecules* **2009**, *10*, 2571−2576.
(26) Tanpichai, S.; Quero, F.; Nogi, M.; Yano, H.; Young, R. J.; Lindström, T.; Sampson, W. W.; Eichhorn, S. J. *Biomacromolecules* **2012**, *13*, 1340−1349.
(27) Sehaqui, H.; Zhou, Q.; Ikkala, O.; Berglund, L. A. *Biomacromolecules* **2011**, *12*, 3638−3644.
(28) Eichhorn, S. J.; Dufresne, A.; Aranguren, M.; Marcovich, N. E.; Capadona, J. R.; Rowan, S. J.; Weder, C.; Thielemans, W.; Roman, M.; Renneckar, S.; Gindl, W.; Veigel, S.; Keckes, J.; Yano, H.; Abe, K.; Nogi, M.; Nakagaito, A. N.; Mangalam, A.; Simonsen, J.; Benight, A. S.; Bismarck, A.; Berglund, L. A.; Peijs, T. *J. Mater. Sci.* **2010**, *45*, 1−33.
(29) Siró, I.; Plackett, D. *Cellulose* **2010**, *17*, 459−494.
(30) Decher, G. *Science* **1997**, *277*, 1232−1237.
(31) Hammond, P. T. *Adv. Mater.* **2004**, *16*, 1271−1293.
(32) Von Klitzing, R. *Phys. Chem. Chem. Phys.* **2006**, *8*, 5012−5033.
(33) Priolo, M. A.; Gamboa, D.; Grunlan, J. C. *ACS Appl. Mater. Interfaces* **2010**, *2*, 312−320.
(34) Priolo, M. A.; Gamboa, D.; Holder, K. M.; Grunlan, J. C. *Nano Lett.* **2010**, *10*, 4970−4974.
(35) Priolo, M. A.; Holder, K. M.; Greenlee, S. M.; Grunlan, J. C. *ACS Appl. Mater. Interfaces* **2012**, *4*, 5529−5533.
(36) Svagan, A. J.; Åkesson, A.; Cárdenas, M.; Bulut, S.; Knudsen, J. C.; Risbo, J.; Plackett, D. *Biomacromolecules* **2012**, *13*, 397−405.
(37) Yang, Y.-H.; Haile, M.; Park, Y. T.; Malek, F. A.; Grunlan, J. C. *Macromolecules* **2011**, *44*, 1450−1459.
(38) Yang, Y.-H.; Bolling, L.; Haile, M.; Grunlan, J. C. *RSC Adv.* **2012**, *2*, 12355−12363.
(39) Gua, C.-H.; Wanga, J.-J.; Yua, Y.; Suna, H.; Shuaia, N.; Weia, B. *Carbohydr. Polym.* **2013**, *92*, 1579−1585.
(40) Rodahl, M.; Hook, F.; Krozer, A.; Brzezinski, P.; Kasemo, B. *Rev. Sci. Instrum.* **1995**, *66*, 3924−3930.
(41) Aulin, C.; Varga, I.; Claesson, P. M.; Wågberg, L.; Lindström, T. *Langmuir* **2008**, *24*, 2509−2518.
(42) Sauerbrey, G. *Z. Phys.* **1959**, *155*, 206−222.
(43) Karabulut, E.; Pettersson, T.; Ankerfors, M.; Wågberg, L. *ACS Nano* **2012**, *6*, 4731−4739.
(44) Fall, A. B.; Lindström, S. B.; Sundman, O.; Ödberg, L.; Wågberg, L. *Langmuir* **2011**, *27*, 11332−11338.
(45) Karabulut, E.; Wågberg, L. *Soft Matter* **2011**, *7*, 3467−3474.
(46) Bieker, P.; Schönhoff, M. *Macromolecules* **2010**, *43*, 5052−5059.
(47) Sun, B.; Jewell, C. M.; Fredin, N. J.; Lynn, D. M. *Langmuir* **2007**, *23*, 8452−8459.
(48) Hansen, N. M.; Plackett, D. *Biomacromolecules* **2008**, *9*, 1493−1505.
(49) Crank, J. *Mathematics of Diffusion*; Clarendon Press: Oxford, U.K., 1967.
(50) Meszaros, R.; Thompson, L.; Bos, M.; de Groot, P. *Langmuir* **2002**, *18*, 6164−6169.
(51) Meszaros, R.; Varga, I.; Gilanyi, T. *Langmuir* **2004**, *20*, 5026−5029.
(52) Dunlop-Jones, N. In *Paper Chemistry*; Roberts, J. C., Ed.; Blackie & Sons Ltd: London, 1991; pp 76−96.
(53) Podsiadlo, P.; Kaushik, A. K.; Arruda, E. M.; Waas, A. M.; Shim, B. S.; Xu, J.; Nandivada, H.; Pumplin, B. G.; Lahann, J.; Ramamoorthy, A.; Kotov, N. A. *Science* **2007**, *318*, 80−83.
(54) Rindlav-Westling, Å.; Stading, M.; Hermansson, A.-M.; Gatenholm, P. *Carbohydr. Polym.* **1998**, *36*, 217−224.
(55) Péroval, C.; Debeaufort, F.; Depré, D.; Voilley, A. *J. Agric. Food Chem.* **2002**, *50*, 3977−3983.
(56) Zhang, P. Y.; Whistler, R. L. *J. Appl. Polym. Sci.* **2004**, *93*, 2896−2902.